ACS APPLIED MATERIALS & INTERFACES

Research Article

www.acsami.org

Site-Selective Modification of Cellulose Nanocrystals with Isophorone Diisocyanate and Formation of Polyurethane-CNC Composites

Natalie M. Girouard,[†] Shanhong Xu,[‡] Gregory T. Schueneman,[§] Meisha L. Shofner,[∥,⊥] and J. Carson Meredith*[,†,⊥]

[†]School of Chemical and Biomolecular Engineering, [∥]School of Materials Science and Engineering, and [⊥]Renewable Bioproducts Institute, Georgia Institute of Technology, Atlanta, Georgia, United States

[‡]National Institute of Standards and Technology, Gaithersburg, Maryland, United States

[§]Forest Products Laboratory, U.S. Forest Service, Madison, Wisconsin, United States

Supporting Information

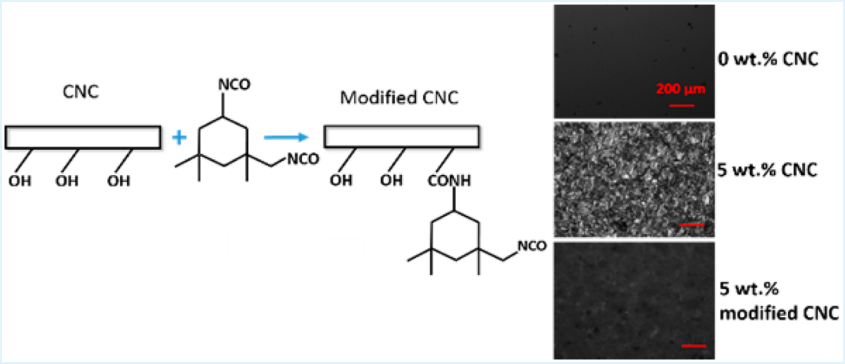

ABSTRACT: The unequal reactivity of the two isocyanate groups in an isophorone diisocyante (IPDI) monomer was exploited to yield modified cellulose nanocrystals (CNCs) with both urethane and isocyanate functionality. The chemical functionality of the modified CNCs was verified with ATR-FTIR analysis and elemental analysis. The selectivity for the secondary isocyanate group using dibutyl tin dilaurate (DBTDL) as the reaction catalyst was confirmed with ^{13}C NMR. The modified CNCs showed improvements in the onset of thermal degradation by 35 °C compared to the unmodified CNCs. Polyurethane composites based on IPDI and a trifunctional polyether alcohol were synthesized using unmodified (um-CNC) and modified CNCs (m-CNC). The degree of nanoparticle dispersion was qualitatively assessed with polarized optical microscopy. It was found that the modification step facilitated superior nanoparticle dispersion compared to the um-CNCs, which resulted in increases in the tensile strength and work of fracture of over 200% compared to the neat matrix without degradation of elongation at break.

KEYWORDS: *cellulose nanocrystal, nanoparticle modification, isocyanate chemistry, thermal stability, polyurethane, polymer nanocomposite, dispersion, mechanical properties*

INTRODUCTION

Cellulosic materials have enjoyed a rich history in commercial applications such as paper, textiles, ropes, and fibers.[1,2] The widespread use of cellulose is owed to its ubiquity in nature, being the most abundant biopolymer produced by our planet.[3] In more recent years, cellulosic hierarchical structures have attracted interest in a variety of research fields.[1] By exploiting the selective hydrolysis of the amorphous domains of ordered cellulose, nanometer-sized crystalline fibers can be extracted from a variety of natural and sustainable sources, including plants, tunicates, and bacteria.[4] Such fibers are currently referred to as cellulose nanocrystals, or CNCs. These highly crystalline fibers have gained commercial interest through pilot-scale production facilities in the United States, Canada, and Europe.[5] The current interest and large-scale production owes itself to the many attractive features of CNCs, namely, renewability and availability, high specific strength, lightweight, and hydroxyl surface chemistry.[1] CNCs have found applications in emulsion stability, polymer composites, packaging and food additives, drug delivery, and flame retardants.[6−10] However, there are some key drawbacks to utilizing this material in other meaningful ways, specifically their comparatively lower thermal stability and hydrophilicity.[11] Therefore, there has been great interest in utilizing their hydroxyl surface chemistry to introduce new functionality to these nanoparticles. There are many examples in literature of cellulose modification routes.[12]

Received: November 9, 2015
Accepted: December 29, 2015
Published: December 29, 2015

DOI: 10.1021/acsami.5b10723
ACS Appl. Mater. Interfaces 2016, 8, 1458−1467

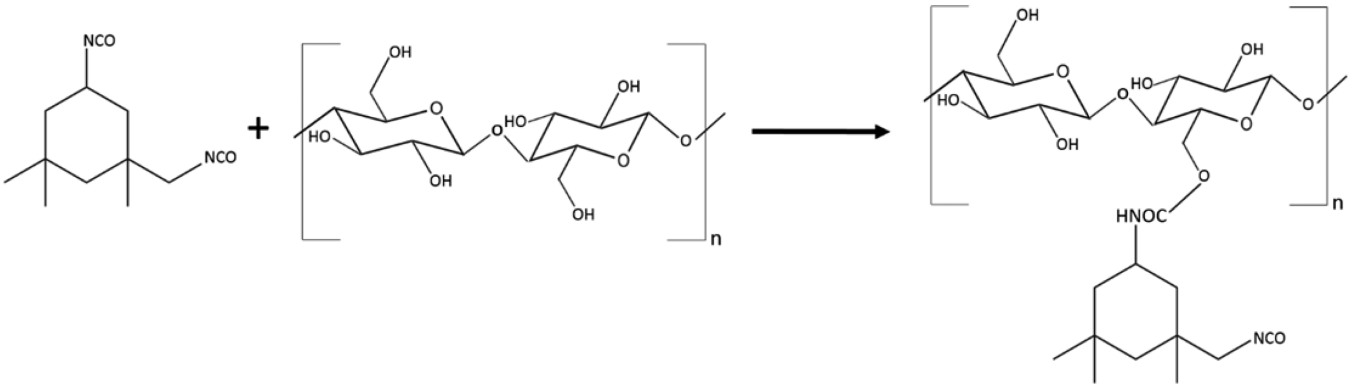

Figure 1. Illustration of IPDI/CNC reaction with the secondary NCO group on IPDI.

For example, poly[(2-dimethylamino)ethyl methacrylate] (PDMAEMA) was grafted onto the CNC surface for the purpose of stabilizing o/w emulsions,[10] and silylation of the −OH surface with *N*-(*β*-aminoethyl)-*γ*-aminopropyltrimethoxysilane was used to improve the compatibility of CNCs with an unsaturated polyester resin.[13] The work presented here explored a modification route using hydroxyl/isocyanate chemistry with isophorone diisocyanate (IPDI) as the reactive monomer. Similarly, hexamethylene diisocyanate (HDI) was used to modify CNCs, and then the modified nanoparticles were incorporated into the segmented thermoplastic polyurethane matrix.[14] The grafted HDI chains linked the CNCs together, for example, chain extension, to form an interconnected network due to the in situ polymerization of the HDI, because both HDI isocyanate groups reacted with cellulose hydroxyl groups.[14] Alternatively, in this work, the proposed modification route did not lead to chain extension of the nanoparticles and offers a unique functionality for CNCs that opens the door for utilizing the isocyanate-modified CNCs in composites with many different polymer matrices.

The polyurethane industry is lucrative and diverse, with reported revenues in 2013 of $25.6 billion and polyurethanes find usage in appliance, automotive, building and construction, electronics, sportswear, and packaging industries.[15] Polyurethanes are often applied as coatings, sealants, adhesives, and foams due to their high toughness and abrasion and chemical resistance.[16] Polyurethanes are also encountered in medical applications due to their biocompatibility, nontoxicity, elasticity, and mechanical properties.[17] The extensive choices available for isocyanates and polyols are responsible for polyurethane's wide range of properties and applications, where the physical properties of polyurethane are dependent upon the chemical structure of the starting reactants.[18] For example, the material properties of polyurethanes will depend on the extent of cross-linking as well as the chain length of the polyol where a high degree of cross-linking would yield a rigid polyurethane, and long chain polyols yield flexible polyurethanes. Of course there is a balance between choosing such chemistries for a given application without sacrificing additional mechanical properties. Often engineered nanocomposites are stiffened but not flexible, or flexible but not stiff.[19] For this reason, many types of fillers have been incorporated into polyurethanes to improve their mechanical properties. These fillers include carbon nanotubes,[20,21] layered silcate clays,[19] and graphite oxide nanoplatelets.[22] Interest in the development of biobased polyurethanes utilizing vegetable oils and sugars, suggest that reinforcements such as cellulosic nanoparticles would be better matches with polyurethane. The combination of cellulosic nanoparticles and polyurethane can aid in the development of bio-nanocomposites containing a significant amount of renewable carbon content.[23] However, as mentioned previously, current reports on CNCs in polyurethane film formulations suffered from the undesirable chain extension and agglomeration of the CNCs, which ultimately resulted in a decrease of the tensile strength, strain at break, and work of fracture in the final composites.[14,23] One example of CNCs successfully used to reinforce polyurethane involved a polyurethane foam formulation. Li et al. reported on CNC/polyurethane foam composites based on a polymeric methylene diisocyanate (MDI) that exhibited enhanced mechanical properties at low nanoparticle loadings.[24] In that study, CNCs improved the tensile and compressive mechanical properties. Specifically, the tensile modulus was improved by 227%, and the compressive strength was improved by 270% compared to the neat foam at 1 wt % CNC.[24] The authors confirmed that CNCs were participating in the cross-linking reaction via the isocyanate groups in MDI and attributed the significant increase in mechanical property to CNCs covalently bonded with the polyurethane foam.[24] Given the diversity of isocyanate chemistries available to polyurethane formulations, it is prudent to investigate alternative isocyanate chemistries with the hydroxyl-decorated CNC surface. The procedure outlined in this manuscript provides a route to produce CNC polymer composites where CNCs are first functionalized with isocyanate prior to their covalent addition to the polymer matrix.

IPDI is part of a class of aliphatic isocyanates used in polyurethane coating applications. Aliphatic isocyanates make up a small percentage of the total isocyanate market, but they are well-known for their high abrasion resistance and resistance to UV degradation.[25,26] These attributes makes these materials attractive for exterior coating applications, such as airplanes. The two most common aliphatic isocyanates are IPDI and HDI. HDI has a linear hydrocarbon backbone with two terminating isocyanate groups on each end. IPDI is an aliphatic ring with one primary and one secondary isocyanate group. In HDI, the two isocyanate groups are of equal reactivity, whereas the isocyanate groups in IPDI are of unequal reactivity.

In the IPDI molecule, the secondary isocyanate (the −NCO substituent directly connected to the ring) has a higher reactivity compared to the primary group (the $-CH_2NCO$ group), which is attributed to the primary group being more sterically hindered by the neighboring methyl group.[27] Moreover, the selectivity for the secondary isocyanate reaction can be enhanced by using dibutyl tin dilaurate (DBTDL) as the

DOI: 10.1021/acsami.5b10723
ACS Appl. Mater. Interfaces 2016, 8, 1458−1467

reaction catalyst and can be inverted to be primary selective by using 1,4-diazabicyclo[2.2.2]octane (DABCO).[27−30] By exploiting this unequal reactivity, it is possible to produce isolated CNCs decorated with IPDI monomers with a pendant isocyanate group that do not chain extend into isocyanate-linked CNC agglomerates. This reaction schematic is given in Figure 1.

The surviving pendant isocyanate group is then available for reaction with additional monomers of interest, such as polyols commonly used in polyurethane formulations. This chemistry can facilitate covalent bonding between the CNC and polymer matrix, a feature that could offer desirable mechanical properties and new functionalities to CNC composites. Such benefits could facilitate accelerated commercialization of these biobased nanomaterials. In this work, CNCs were successfully modified with IPDI, and for demonstrational and performance based-comparative purposes, modified CNC (m-CNC) and unmodified (um-CNC) particles were incorporated into a polyurethane elastomer using IPDI as the isocyanate-containing monomer and cross-linked with a polyether-based triol.

MATERIALS AND METHODS

Freeze-dried CNCs (FD-CNCs) were provided by the U.S.D.A. Forest Products Laboratory and used as received. The CNCs were freeze-dried from an aqueous CNC suspension prepared from mixed southern yellow pine dissolving pulp via 64% sulfuric acid digestion as described in detail elsewhere.[31] The resulting CNCs had sulfate functionality due to residual sulfate esters on their surfaces. The CNCs were determined to contain 0.96 wt % sulfur on a dry cellulose basis by inductively coupled plasma/optical emission spectroscopy (ICP/OES).[32] The counterion on the nanocrystals was Na^+. The CNC dimensions were analyzed by TEM, and the experimental details are given in the Supporting Information (Figure S1). IPDI was purchased from Sigma-Aldrich at 98% purity and used as received. The IPDI was stored at 4 °C. The cross-linker used in polymer synthesis was a polyether polyol provided by Bayer MaterialScience (LHT-240, Molecular Weight = 700 g/mol). Solvents of anhydrous dimethyl sulfoxide (DMSO) and toluene were purchased from Sigma-Aldrich and used as received. Isocyante catalysts, DBTDL, and DABCO, were purchased from Sigma-Aldrich and used as received.

Surface Modification. The FD-CNCs were first mixed with DMSO by magnetic stirring for 30 min. The concentration of CNC in DMSO was ∼3 wt %. This mixture was then sonicated for 1 h with a 2510 Branson bath sonicator. A separate vessel partially submerged in an oil bath containing IPDI was heated to 60 °C under a flowing nitrogen atmosphere. The DBTL was then added to the IPDI and allowed to stir for 5 min. The FD-CNC/DMSO suspension was added dropwise to the stirring IDPI/DBTDL mixture with a separatory funnel. The reaction proceeded overnight in a flask with N_2 inlet and outlet ports. The reaction was run in excess of IPDI at a weight ratio of IPDI to CNC of 67:1. After the reaction, the mixture was washed with toluene and centrifuged at 2800 rpm for 3 min, and repeated 3 times. The toluene was poured off, and the CNCs were either mixed with triol for composite synthesis or allowed to dry in a vacuum oven overnight. An identical procedure was applied to produce the m-CNCs using DABCO as the reaction catalyst. All m-CNC characterizations were performed on samples that were synthesized using DBTDL as the reaction catalyst, with the exception of ^{13}C NMR, which was employed to compare the selectivity of the two catalysts studied here.

Polyurethane Film Preparation. Composites were synthesized with both m-CNCs and um-CNCs at loadings of 1 and 5 wt %, and DBTDL was used as the reaction catalyst for both the m-CNC preparation and the polyurethane film formulation. Elemental analysis was used to calculate the relative weight ratios of IPDI and CNC in the m-CNCs. This information was used to estimate the equivalent weight of CNC in the m-CNC sample, and all composite loadings were based on the weight of CNC only. All polymers were synthesized with a 1:1 stoichiometric ratio of −NCO from IPDI and −OH from triol. The concentration of −NCO groups on the modified CNCs was taken into account by the experimental values given by elemental analysis. The um-CNCs were first mixed with toluene and then sonicated. For both types of CNC composites, the CNC/toluene mixture was magnetically stirred with triol for 30 min and then vacuum oven-dried until there was no mass change, indicating that the toluene had been removed. The CNC/triol mixture was then stirred with DBTDL for a few minutes. IPDI was added to the mixture was allowed to magnetically stir for 30 min. The nanocomposite mixture was then poured onto a hydrophobic glass substrate and casted to the desired thickness with a doctor blade. The polymer was cured at 100 °C in a vacuum oven for 2 h. For comparative purposes, a neat polyurethane polymer film was synthesized. The procedure for producing the neat polymer was identical to the procedure for the composite, except that in the step where the CNC/toluene mixture was added to the triol, here only toluene was added.

Attenuated Total Reflectance Fourier Transform Infrared Spectroscopy. The chemical structure of the um-CNCs, m-CNCs, and polymer films was analyzed with ATR-FTIR using an ATR accessory (Bruker Platinum ATR) with a Bruker Vertex 80 V spectrometer. The ATR was equipped with a germanium crystal plate, which had a spectral range of 10 000 to 10 cm^{-1}. The spectra were corrected to subtract the background signals and flatten the baseline. The wavenumber scan range was from 4000 to 600 cm^{-1} with a resolution of 4 cm^{-1} and a total of 64 scans. For the um-CNC/m-CNC comparison, the 1060 cm^{-1} band was chosen as the normalization wavenumber since this absorbance was associated with ether functional groups, which were assumed to not participate in the reaction. Similarly, the composite spectra were normalized by a functional group assumed to not participate in the cross-linking reaction, the 1380 cm^{-1} peak,[33] which was assigned to the dimethyl group on the C3 carbon of the aliphatic ring in the IPDI monomer.[29]

Elemental Analysis. Modified and unmodified CNC samples were sent to ALS Environmental in Tuscon, AZ, for elemental analysis. The samples were analyzed for C, H, O, and N content. The C, H, and N analysis was performed on a PerkinElmer 2400 Series II, and the O analysis was performed on a Leco Truspec Analyzer. The PerkinElmer instrument was calibrated with acetanilide, and the Leco Truspec was calibrated with benzylic acid. Approximately 2 to 5 mg of sample was weighed and then held in the combustion chamber for about 5 min. The oxygen analyzer was held at 1000 °C and the C, H, N analyzer was held at 935 °C. The degree of substitution was calculated based on the nitrogen content.

Nuclear Magnetic Resonance Spectroscopy. The selectivity for the primary/secondary isocyanate group using DABCO and DBTDL catalysts was verified with solid-state ^{13}C NMR. Approximately 50 mg of um-CNC and m-CNC was packed into a 24 mm OD MAS rotor. CP-MAS spectra were recorded using a Bruker AV3−400 NMR spectrometer operating at a ^1H frequency of 400 MHz. A dual-channel BB-MAS probe was operated at a spinning speed of 10 kHz. Cross-polarization was achieved with a trapezoidal shaped contact pulse for ^1H varying in power from 70 to 100% and a length of 2 ms. Repetition delay between scans was 4 s, and at least 12 000 scans were acquired for each sample to measure spectra with an excellent signal-to-noise ratio. The spectra were normalized by the peak positioned at δ = 75 ppm, an absorbance that was attributed to the C2, C3, and C5 carbons in the crystalline cellulose.[34] These groups were assumed to not participate in the reaction.

Thermogravimetric Analysis. Thermal stability and changes in degradation patterns associated with the modification step were assessed with thermogravimetric analysis (TGA; TA Instruments TGA Q5000). Samples were heated from room temperature to 600 °C at a rate of 5 °C/min under a flowing nitrogen atmosphere. The onset temperature (T-onset) and temperature at maximum weight loss rate (T-max) were determined with TA Universal Analysis software. The onset temperature of degradation was assessed by TA Universal Analysis software by manually choosing a point before and after the sharp drop in mass loss on the weight loss curve. The temperatures at maximum weight loss were determined for each event of degradation

DOI: 10.1021/acsami.5b10723
ACS Appl. Mater. Interfaces 2016, 8, 1458−1467

with TA Universal Analysis software by manually selecting a point before and after the peak maximum on the derivative weight loss curve. Measurements were repeated three times, and average values were reported.

Polarized Light Microscopy. CNC dispersion in the polyurethane matrix was investigated qualitatively by the observation of birefringence with an optical microscope (Olympus BX51) equipped with two polarizers (Olympus U-AN360P). Images were captured with an Olympus camera (U-CMAD3) and processed with PictureFrame software. All films were imaged in transmission mode with a 20X objective and at full extinction of the polarizers.

Tensile Testing. Uniaxial tensile testing was performed using an Instron 5842. The samples were prepared by cutting the films with a dog bone die based on the ASTM standard D1708−13. The test section was ∼22 mm long, and samples were ∼0.6 mm thick. The testing speed used was 10 mm/min. Material properties associated with changes in tensile strength measured at break, percent elongation, and work of fracture were reported. A minimum of four samples were tested for each material composition, and the average values were reported.

RESULTS

CNCs can have dimensions ranging from 50 to 500 nm long and from 3 to 5 nm wide.[1] Given these dimensions, CNCs have aspect ratios ranging from 10 to 167, although the specific values depend on the source and reaction conditions.[2] Wood-based CNCs are reported to have dimensions ranging from 100 to 200 nm in length and 3−5 nm in width.[2] A representative TEM image from the aqueous-based CNC suspension used in this study can be found in the Supporting Information (Figure S1). The rodlike/whisker morphology and the geometric dimensions were consistent with data reported in the literature for CNCs obtained from wood.[31]

To verify the attachment of the IPDI monomer to the CNC surface with pendant isocyanate groups, as illustrated in Figure 1, ATR-FTIR was used to characterize the m-CNCs and um-CNCs. The isocyanate functionality has an isolated and strong absorbance around 2240 cm^{-1};[33] thus, evidence of its presence in any of the samples tested should be obvious. After the m-CNCs were washed with toluene three times, the supernatant of the third centrifuged product was tested. The ATR-FTIR results indicated (Supporting Information, Figure S2) that a negligible amount of isocyanate was remaining from the reaction mixture after the toluene washing; thus, the isocyanate peak observed in the modified particles would be largely due to the presence of isocyanate on the CNC particles. Figure 2 shows the ATR-FTIR spectra for the um-CNC and m-CNC. The um-CNCs showed IR absorbances characteristic of cellulosic functional groups. There were strong absorbances around 3000−3550 cm^{-1} and 900−1100 cm^{-1}, the bands assigned to −OH and −C−O−C vibrations, respectively.[14,33] Changes across all regions of the spectra were observed for the m-CNCs; the most significant changes will be discussed. First, there was an apparent decrease in the −OH peak, which indicated that some of these functional groups were consumed. This decrease in the −OH peak coupled with the appearance of the isocyanate band at 2240 cm^{-1} gave a strong indication that the CNC surface was successfully modified. Additionally, there were significant increases in the absorbance of the carbonyl bond present in urethane groups at 1500−1750 cm^{-1}.[14,33] These results suggested that not only was the CNC surface successfully modified with the IPDI monomer but also only some of the isocyanate groups were attached, thus demonstrating the unequal reactivity of the IPDI. The available isocyanate group from the m-CNC particles may facilitate a route for further CNC modifications and/or a covalent linkage with the polymer matrix.

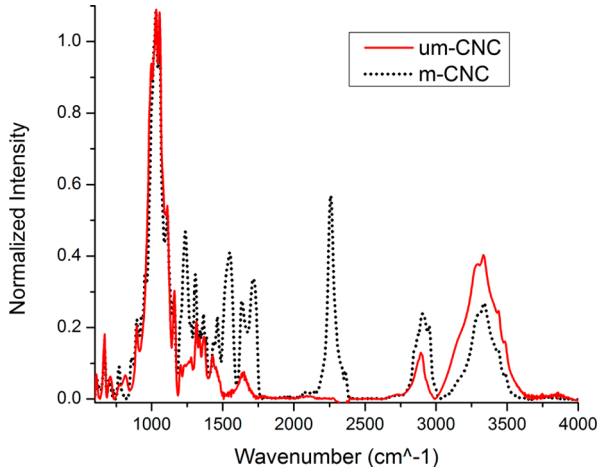

Figure 2. ATR-FTIR spectra of um-CNCs and m-CNCs.

The degree of substitution (DS) is a parameter used to describe the extent of modification and specifically translates to the number of hydroxyl groups that have been modified per one anhydroglucose unit (AGU). The results of the elemental analysis are given in Table 1, and these data were used to calculate the DS for the modification of CNCs with IPDI.

Table 1. Elemental Composition of um-CNCs and m-CNCs

	C	H	N	O
unmodified CNC (wt %)	41.1	5.6	<0.05	44.4
modified CNC (wt %)	50.3	7.0	5.2	31.0

The unmodified cellulose contained a negligible amount of nitrogen, as expected. The modified CNCs contained 5.23 wt % nitrogen, indicating that the IPDI was present. The DS was determined by considering the theoretical percentage of nitrogen that would be present in the modified CNCs if one IPDI monomer was attached to the three hydroxyl groups available in one AGU, the maximum DS.[35] The total molecular weight of such a structure would be 831 g/mol, and the % nitrogen would be 10%. Comparing the theoretical value, 10%, to the measured value of % nitrogen, 5.23%, the DS was ∼0.52, which corresponds to 17% of the hydroxyls participating in the reaction. This value reflects the DS for bulk CNC; however, not all of the CNC hydroxyls are expected to react. Typically it is more appropriate to consider a DS for the surface since it is the surface hydroxyls that would participate in the reaction. Therefore, if only the surface hydroxyls of the CNC are considered, the DS would be higher. The DS for the surface is noted by DS_{surf}.

In their review article, Eyley et al. give an equation to calculate the number hydroxyl groups on the CNC surface in moles per gram, a value that is then used in a separate equation to calculate DS_{surf}.[12] Using the dimensions of the CNCs used in this work, the CNC crystallographic parameters reported by Wu et al.,[36] and the elemental analysis data, the DS_{surf} was calculated to be 1.4. The DS_{surf} can be related to DS by the chain ratio parameter, R_c, which is the ratio of exposed cellulose chains to the total number of chains in a CNC.[12] Using the calculated value of DS_{surf} = 1.4, and the calculated R_c value for the CNCs used in this work, the DS was calculated to be 0.51.

DOI: 10.1021/acsami.5b10723
ACS Appl. Mater. Interfaces 2016, 8, 1458−1467

This value was similar to the DS calculated using the elemental analysis data and molecular weight arguments, and was therefore considered appropriate. A more detailed description of the equations used to calculate DS and DS_{surf} can be found in the Supporting Information.

Eyley et al. noted that the maximum theoretical DS_{surf} is 1.5 due to the crystalline structure of CNCs where one C6, C3, and C2 hydroxyl group point out of the face of the crystal for every cellulose repeat unit (2 AGUs).[12] Given this information, the DS_{surf} calculated in this work was relatively high. The authors also noted that $DS_{surf} > 1$ was unlikely given the assumed lack of reactivity of the C3 hydroxyl group, and that $DS_{surf} > 1$ would disrupt the crystalline structure of cellulose.[12] The integrity of the crystalline structure after modification was qualitatively assessed with ^{13}C NMR, and it is discussed below.

In addition to characterizing the surface chemistry, the crystallinity of the CNCs was also characterized. There are many ways to determine the crystallinity of CNCs, the most common being the XRD peak height method; however, this method often overestimates the crystallinity.[37] Other methods involving XRD include peak deconvolution or an amorphous peak subtraction method, each of which calculate a lower degree of crystallinity compared to the XRD peak height method.[37] Although it is a less common technique, ^{13}C NMR can also be used to determine CNC crystallinity.[37,38] The values mentioned here were used for comparing the degree of crystallinity of the um-CNC to the m-CNC products. In the NMR spectra, the C4 peak in the range of δ = 93−87 ppm was assigned to the crystalline form of cellulose, and its shoulder peak at δ = 86−80 ppm was assigned to the amorphous regions of cellulose.[37,38] The crystallinity index, CI, is computed with ^{13}C NMR by integrating the C4 crystalline peak and dividing that value by the total area of the C4 peak (δ = 93−80).[37,38] Upon integration of these peaks, it was determined that the CI of um-CNC was 67%, and for both m-CNC products the CI was 66%. Although discrepancies are expected with CI values for CNCs given the variety of experimental techniques, cellulose sources, and CNC extraction methods available, the CI reported here fell within the range of the expected value for CNCs, which is 54−88% crystallinity.[1] In any case, these data show that it can be reasonably determined that the modification step did not result in a significant disruption of the CNC crystalline structure as suggested by Eyley et al. Possible explanations of the high DS_{surf} could be due to a lack of understanding of the CNC surface on the atomic scale. For example, the exact nature of the CNC crystal structure is not well-understood, as some researchers have proposed a region in cellulose of intermediate order and mobility compared to the crystalline and amorphous domains.[39] If so, such a "para-crystalline" region could accommodate additional IPDI groups and could result in a higher DS_{surf} than expected. Another possibility could be the method in which the CNCs are modified, specifically with significant excess of the IPDI reactant, and with a CNC swelling solvent such as DMSO. When CNCs were modified in dimethylformamide (DMF) with HDI in a 5:1 excess of HDI, the DS was calculated to be 0.45 by elemental analysis, a similar value reported here.[14] The discussion presented here is meant to put into perspective the possibilities for the extent of surface coverage in CNC modifications and highlight important considerations of such chemical modifications, specifically, crystallinity. Although the DS_{surf} was higher than expected, it was difficult to say with certainty the extent of modification to the CNC surface given the assumptions of the number of hydroxyl groups on the surface and an incomplete picture of the CNC surface mobility and crystallinity. Therefore, it is perhaps more appropriate to report a range of DS from 0.5 to 1.4. Overall, these data indicated that the IPDI modification of CNCs resulted in good surface coverage without compromising the CNC crystallinity.

^{13}C NMR analysis also gave insight into the selectivity of two isocyanate catalysts, namely, DBTDL and DABCO. The normalized spectra for the um-CNCs and m-CNCs modified using DBTDL and DABCO catalysts are given in Figure 3. The

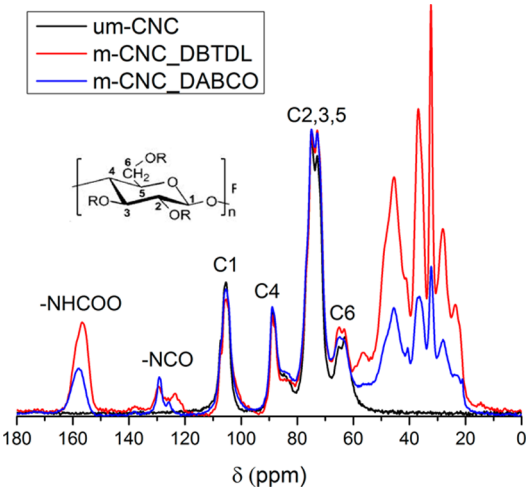

Figure 3. ^{13}C NMR spectra for um-CNCs and m-CNCs catalyzed with DBTDL and DABCO.

spectrum for the um-CNC represented a typical solid-state ^{13}C NMR spectra for crystalline cellulose.[34] Major peaks in Figure 3 are labeled according to the corresponding six carbons in one AGU.[14,34] Changes to the NMR spectra associated with the IPDI modification were observed. In addition, it was possible to observe differences in the m-CNC spectra depending on the type of catalyst used for the preparation. First, both m-CNC spectra showed new peaks in the δ = 160 to 120 ppm range, and in the δ = 50 to 20 ppm range when compared to the um-CNCs. Peaks in the δ = 50 to 20 ppm region were due the hydrocarbons present in the IPDI, specifically, $-CH_2-$ from the aliphatic IPDI ring (δ = 45.5 ppm), the tertiary carbon (δ = 36.9 and δ = 32.3 ppm), and the $-CH_3$ groups (δ = 28.0 and δ = 23.5 ppm). The peaks in the δ = 160 to 120 ppm region represented the urethane (δ = 158.0−156.8 ppm) and isocyanate (δ = 129.2−123.4 ppm) functionality on the CNC particle. All chemical shift values were consistent with previously established values.[14,33,40]

From solution NMR it is well-known that the primary urethane linkage (δ = 157.13 ppm)[29] has a higher chemical shift than the secondary urethane linkage (δ = 155.99 ppm).[29] The observation of distinct peaks for the primary and secondary urethane assignment was less apparent due to the broader lines encountered in solid-state NMR. However, the selectivity of the catalysts can be inferred by the apparent chemical shift of the single urethane peak, which in fact must be a superposition of two broader peaks. The urethane peak was positioned at δ = 158 ppm for the DABCO catalyst and at δ= 156.6 ppm for the DBTDL catalyst. Hence, the DABCO catalyst had a higher affinity for the primary isocyanate reaction site.

Alternatively, two distinct peaks were observed in the solid-state NMR spectra for the assigned isocyanate absorbance.

DOI: 10.1021/acsami.5b10723
ACS Appl. Mater. Interfaces 2016, 8, 1458−1467

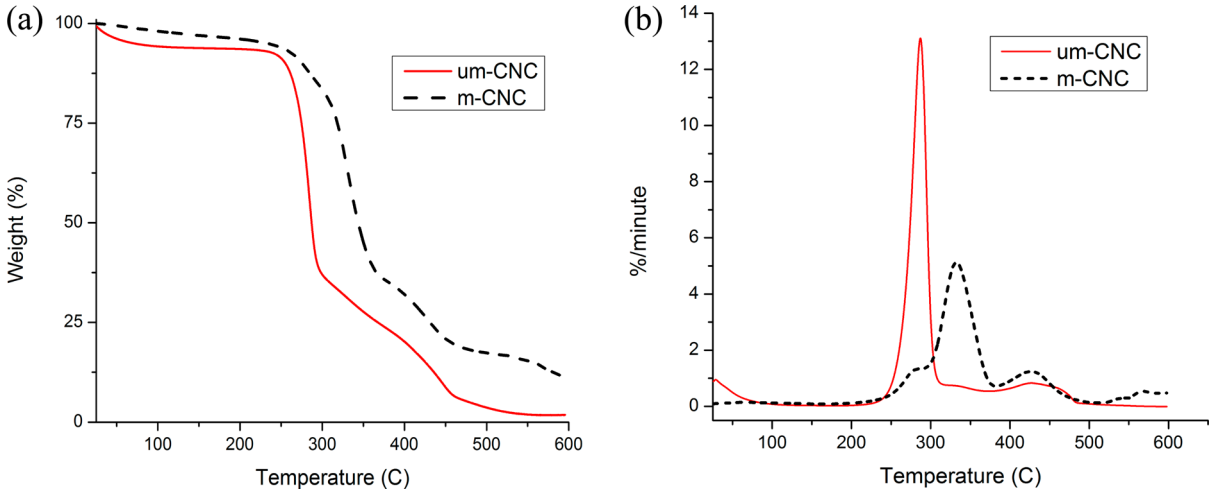

Figure 4. Weight loss curves (a) and (b) derivative weight loss curves for um-CNCs (----) and m-CNCs (- - -).

From solution NMR, it is known that the primary isocyanate group (δ = 122.22 ppm)[29] has a lower chemical shift compared to the secondary isocyanate site (δ = 122.98 ppm).[29] Similar results were found here when the neat IPDI was tested by solution ^{13}C NMR (Supporting Information, Figure S4). The primary isocyanate was positioned at 121.9 ppm, and the secondary isocyanate was at 123.8 ppm. The secondary peak also showed a stronger absorbance in this spectra, and the ratio of the secondary to primary peak intensity was 1.50. To compare the relative quantities of primary and secondary isocyanates in the solid-state ^{13}C NMR spectra, however, the peak area should be considered.[34] This information was used to infer the selectivity of the two catalysts. First, the CNCs modified using the DABCO catalyst indicated two isocyanate peaks at 125.8 and 129.4 ppm, and the CNCs modified using the DBTDL catalyst indicated isocyanate peaks positioned at 123.5 and 129.2 ppm. On the basis of the values established by solution NMR for the assignment of primary and secondary isocyanate peaks, it was assumed that the peak at ∼124 ppm corresponded to the primary isocyanate, and that the peak at ∼129 ppm corresponded to the secondary isocyanate. Given the relative area under the curve of the primary and secondary isocyanate peaks, it was apparent that the DABCO catalyst preferentially reacted the primary isocyanate. Specifically, the integrated peak area ratio of the secondary to primary isocyanate was 3.63 for the DABCO catalyst compared to 0.81 for the DBTDL catalyst. ^{13}C NMR suggested that the catalyst choice impacted the selectivity for an −OH cellulose reaction with either primary or secondary isocyanate groups. These results, along with the ATR-FTIR and elemental analysis data, confirmed that the m-CNCs had both isocyanate and urethane functionality.

Another qualitative difference between the two catalysts was revealed by the noticeable differences in intensity after the data was normalized to represent equivalent amounts of unmodified cellulose. The CNCs modified using the DBTDL catalyst showed peaks of higher intensity in the urethane region and in the region representing the aliphatic carbons from the IPDI. This result indicated that the DBTDL catalyst facilitated a higher grafting density of IPDI molecules to the CNC surface when compared to the DABCO catalyst. It was determined that the DBTDL catalyst was more efficient than DABCO for the reaction studied here. Intuitively, this result was not surprising considering that the DABCO catalyst selects for the inherently less reactive isocyanate. Data reported by Speier et al. indicated a similar conclusion with the calculated reaction rate constant for the secondary isocyanate using DBTDL occurring approximately twice as fast as the reaction rate for the primary isocyanate using DABCO.[30] Additionally, the authors reported that the reaction catalyzed by DBTDL reached 100% conversion sooner than the reaction catalyzed by DABCO, with a 2:1 NCO/OH stoichiometry and a temperature of 20 °C.[30]

To compare the thermal degradation behavior of the um-CNCs and m-CNCs, the materials need to be dried in a similar manner prior to TGA experiments since previous results have shown that the degradation behavior was related to the drying method used.[41] After the CNCs were functionalized with IPDI, the particles were washed with toluene to eliminate excess reactants and allowed to dry in a vacuum oven at 80 °C. Thus, the um-CNCs were also wet with toluene and dried in a vacuum oven at 80 °C. When comparing the onset of degradation of freeze-dried um-CNC to the m-CNC particles, there were appreciable changes. These changes are shown in the weight loss curves and derivative weight loss curves given in Figure 4. First, the onset of degradation for the m-CNCs was increased. A similar increase in the onset of degradation was also observed by Tang et al. when wood-based CNCs were chemically modified with PDMAEMA[10] and by Pereda et al. when cotton CNCs and starch nanocrystals (SNC) were physically modified with PEO.[42] Here, the m-CNCs began to degrade at 300 °C, a 35 °C increase compared to the um-CNCs. The um-CNCs also began to lose weight much earlier in the heating process (∼35 to 100 °C) than the m-CNCs. This difference was attributed to a small amount (∼6 wt %) of water associated with the um-CNC particles.[10] This moisture is likely not present for the modified particles due to the incorporation of organic molecules on the CNC surface. The m-CNCs also contained more char at the end of the run at 600 °C compared to the um-CNCs, 10 ± 1.8 wt % and 2.3 ± 0.6 wt %, respectively. This result also reflected the improved thermal stability of the m-CNC particles.

To gain insight into the events involved in the degradation process, the derivative TGA curve (Figure 4b) was considered. The degradation of the um-CNCs occurred in two major steps, while the degradation of the m-CNCs occurred in three major steps. These steps were identified by the temperature associated with the maximum slope value in the weight loss signal,

DOI: 10.1021/acsami.5b10723
ACS Appl. Mater. Interfaces 2016, 8, 1458−1467

appearing as a peak in derivative signal. The first temperature at maximum weight loss rate (T-max 1) for both um-CNC and m-CNC was 280 °C. This peak signified the first degradation event for both particles, although this event was more significant for the um-CNCs. This process was attributed to the decomposition of the negatively charged sulfate ester groups on the CNC surface.[43,44] The um-CNCs continued to degrade more slowly with another event occurring at ∼450 °C. This decomposition was attributed to the slower kinetic degradation of the crystalline interior[44] and also occurred for both types of particles. The m-CNCs exhibited an additional mode of degradation at 330 °C. This event was characteristic of hard segment polyurethane (−NHCOO) degradation and has been classified as the decomposition of a urethane group into an isocyanate and alcohol group.[45] These results provided further evidence of the CNC/urethane functionality and demonstrated the improved thermal degradation behavior as a result of the modification.

A summary of the thermal degradation data for the toluene-treated um-CNC and m-CNCs and freeze-dried um-CNC is given in Table 2. Specifically, values for onset temperature of degradation (T-onset) and temperatures at maximum weight loss for each degradation process (T-max 1, T-max 2, and T-max 3) are shown. The freeze-dried CNCs vacuum oven-dried with toluene had a similar T-onset, T-max 1, and T-max 2 compared to the freeze-dried um-CNCs, indicating that the additional washing and drying preparation steps did not have a significant impact on the degradation behavior of the particles. Therefore, it was concluded that the increase in the onset of degradation observed with the m-CNCs was solely due to the modification step and not the drying method or some combination of the two.

Table 2. Thermal Degradation Properties of CNC Particles Prepared by Various Methods

particle:	um-CNC	um-CNC	m-CNC
drying method:	freeze-dry from aqueous	vacuum oven (80 °C) from freeze-dry	vacuum oven (80 °C) from freeze-dry
T-onset (°C)	266 ± 3	265 ± 6	300 ± 1
T-max 1 (°C)	289 ± 0.5	287 ± 1	286 ± 10
T-max 2 (°C)	454 ± 0.1	433 ± 10	329 ± 2
T-max 3 (°C)			426 ± 4

The um-CNC and m-CNC particles were incorporated into a polyurethane elastomer based on IPDI and triol according to the procedure outlined in the Materials and Methods section. The nanoparticle dispersion, polymer chemistry, and mechanical property were assessed with PLM, ATR-FTIR, and tensile testing, respectively. PLM is a useful tool for analyzing CNC dispersions in transparent/amorphous media.[32,46] The CNC particles will appear polychromatic at certain concentrations if arranged in liquid crystalline domains and as white/bright regions if they are randomly oriented and clustered.[1,47] The crystalline character of CNCs affords them an optical anisotropy, giving rise to obvious birefringence when viewed under cross polarizers. Conversely, if the PLM analysis yields uninteresting results (a dark image), it can be concluded that the CNCs are well-dispersed at this length scale. Additionally, PLM can give an indication of the homogeneity of CNC dispersion at larger length scales when compared to electron microscopy techniques considering the viewing area offered by each method. While SEM or TEM may allow the user to see a few square nanometers or micrometers of the sample surface, optical microscopy images are on the order of square millimeters and represent a three-dimensional distribution of the CNCs, thus providing a more complete picture of their dispersion. CNCs are also difficult to image with electron microscopes given their low stability in the electron beam, elemental similarity to most polymer matrices, and ∼5 nm width. Viewing the um-CNC and m-CNC composites between crossed polarizers gave information about the degree of CNC dispersion achieved in the polyurethane composites, and these images are given in Figure 5a. These images were qualitatively compared to the neat polyurethane matrix, in which no birefringence was observed, suggesting a completely amorphous material. The um-CNC composite appeared to have CNC aggregates present across a large area of the sample, while the m-CNC composite showed limited birefringence at identical CNC loadings. This result implied that the m-CNCs were dispersed in the polyurethane matrix on the micrometer scale. Similar results were achieved when CNCs were mixed with a waterborne epoxy system and filler−matrix compatibility was enhanced by physical polymer/nanoparticle interactions.[32] The m-CNCs were likely dispersed more homogeneously in the polyurethane matrix due to increased chemical compatibility

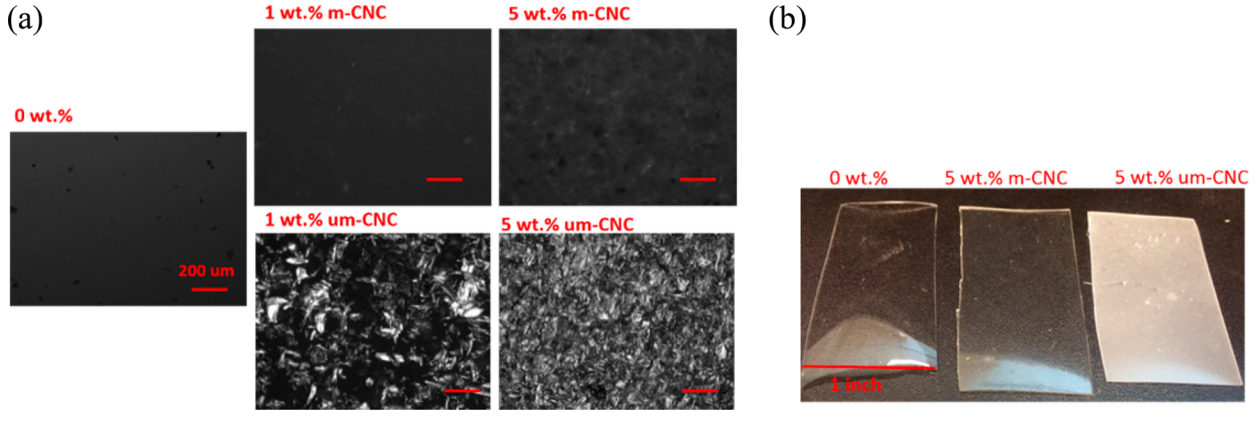

Figure 5. (a) PLM images of cellulose nanocrystal-containing polyurethane composites and neat polyurethane. (b) Photographic image of cured polymers.

DOI: 10.1021/acsami.5b10723
ACS Appl. Mater. Interfaces 2016, 8, 1458−1467

with the monomeric components and the formation of urethane linkages. The m-CNC composite may have achieved better dispersion due to covalent linkage formation between the triol and the pendant isocyanate group on the m-CNC surface. The dispersion levels attained were likely related to the solvent used as well, toluene. Generally, toluene is a poor solvent for CNCs and was used as the dispersing solvent in both composite formulations, given its compatibility with the m-CNCs and volatility that facilitates film formation from solvent-based processing methods. The dispersion of the um-CNC particles in composites could be improved by using a better solvent for CNCs, like DMSO (Supporting Information, Figure S3).

In addition to displaying a stark contrast in the amount of birefringence observed in the polyurethane composites, the bulk composites also had contrasting optical properties. These differences are highlighted by Figure 5b. The sample containing um-CNCs took on the white color of the FD-CNC powders. Comparing the appearance of the m-CNC composite to the um-CNC composite, it was clear that the modified particles had less of an impact on the bulk optical property of the polyurethane sample. Coupling this observation with the polarized light micrographs, it was concluded that the modified CNCs were well-dispersed in the polyurethane matrix and that the enhanced dispersion was due to the modification step.

To assess the effect that CNCs had on polyurethane chemistry, ATR-FTIR was used to characterize the functional groups present in the composites, and the results are summarized in Figure 6. For all concentrations tested here, there was no evidence of isocyanate absorption at 2240 cm^{-1}, thus indicating within the sensitivity of the measurement that all of the IPDI molecules reacted. The band at 1700 cm^{-1} represented the urethane linkage (−NHCOO), and the band at 3330 cm^{-1} represented the secondary amide (−CONH), which typically absorbs in the 3460−3400 cm^{-1} range but is lowered in the solid state and with hydrogen bonding.[33] Additional bands in the fingerprint region (1500−600 cm^{-1}) were similar for all composites and represented a combination of ether, amine, and hydrocarbon bonds.[33] While their identification was not trivial, the CNC loadings used here did not create new bands, and intensities were comparable across all wavenumbers tested here. Therefore, it was assumed that all composites had similar chemistry and similar concentrations of urethane linkages.

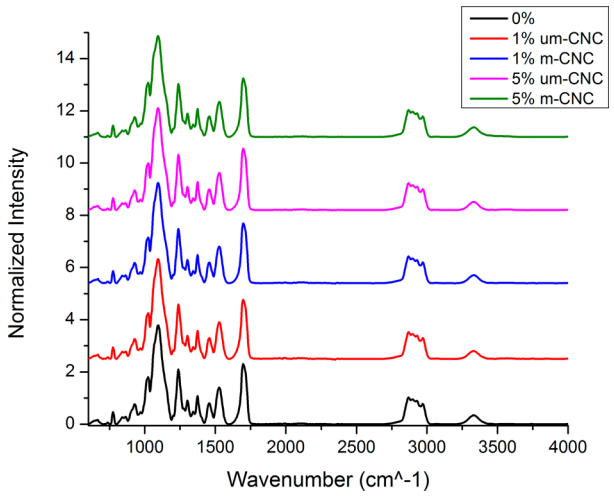

Figure 6. ATR-FTIR spectra for 0, 1, and 5 wt % um-CNC and m-CNC polyurethane composites.

The mechanical performance of the composites compared to the neat matrix was assessed with tensile testing. The elongation at break for all samples tested ranged from 160 to 190%, although all measurements fell within the error ranges of each other (Supporting Information, Figure S5b), so no change in this property was observed with CNC addition. The data for tensile strength at break and work of fracture are given in Figure 7, with error bars representing confidence intervals of 95%. As a general trend, the samples containing m-CNC performed better than samples containing um-CNC at the same concentrations. For example, at a 1 wt % concentration, the m-CNC composite had improved tensile strength and work of fracture by 42% compared to the um-CNCs. This trend was more apparent for the 5 wt % samples, with a 163% increase in tensile strength and a 132% increase in the work of fracture for the m-CNC composites. In fact, the 1 wt % m-CNC samples performed better than the 5 wt % um-CNC samples. Therefore, less of the modified material is needed to achieve a similar or improved mechanical performance when compared to the unmodified particles. Most significantly, the 5 wt % m-CNC sample improved the tensile strength by 226%, and the work of fracture by 257% when compared to the neat matrix, a similar level of reinforcement to CNC/polyurethane foams[24] and polyurethane reinforced with nanosilica particles.[48]

Since the elongation at break was similar for all samples tested (Supporting Information, Figure S5), it is possible that one of the mechanisms of reinforcement was due to the stiffening of the matrix by the CNC particles. While the tensile test standard chosen for this study did not allow for quantitative determination of elastic modulus, the initial slope of the stress−strain curves suggested that it was increased with increasing CNC loadings (Supporting Information, Figure S5). This result was expected given that the CNCs were quite rigid compared to the soft polyurethane matrix[49] ($E_{L\text{-}CNC} \approx 150$ GPa, $E_{PUE} \approx 0.025$ GPa). However, the significant increase in the tensile strength and work of fracture suggested that there was more at work here than stiffening of the matrix. The factors affecting tensile strength and work of fracture include: particle size, particle loading, and the strength of the filler−matrix adhesion.[49] Assuming that for a given concentration of m-CNCs or um-CNCs the effective particle loading and particle size was similar, an increase in the tensile strength would imply good filler−matrix adhesion. The forces behind filler−matrix adhesion can range from physical (electrostatic, mechanical interlocking, van der Waals) to chemical (ionic, metallic, covalent).[48] These results, along with the FTIR and PLM, give evidence for strong m-CNC/polyurethane interactions such as chemical bonding.[48]

CONCLUSIONS

The reaction of freeze-dried CNCs with IPDI was optimized to yield modified cellulose particles with a high surface coverage of the difunctional monomer. ATR-FTIR and ^{13}C NMR confirmed that the particles had both isocyanate and urethane functionality and indicated that the DBTDL catalyst selectively reacted the secondary isocyanate. The pendant primary isocyanate group was then used as a route to facilitate covalent bond formation with a polyurethane elastomer, resulting in a significant improvement in the tensile properties at 5 wt % m-CNC compared to the neat matrix. According to the tensile data, the m-CNCs imparted stiffness to the polyurethane matrix

DOI: 10.1021/acsami.5b10723
ACS Appl. Mater. Interfaces 2016, 8, 1458−1467

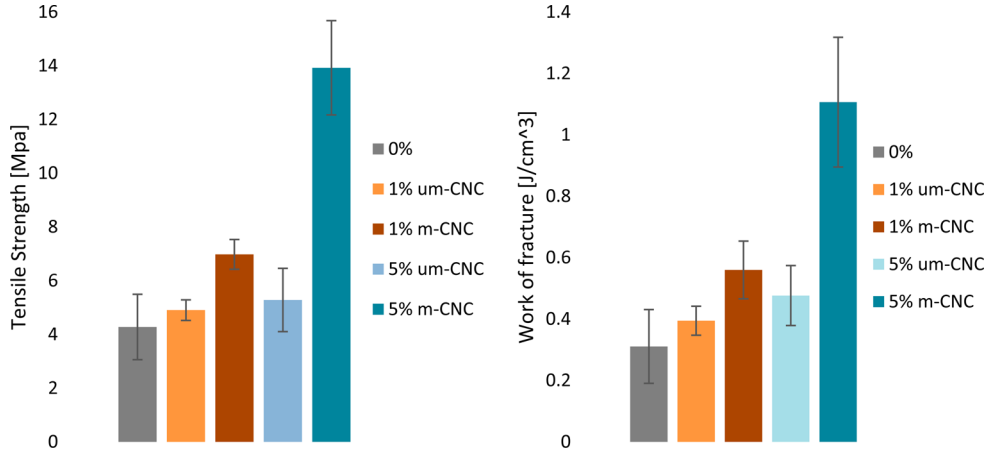

Figure 7. Tensile strength and work of fracture for um- and m-CNC composites and neat polyurethane.

without degrading the flexibility of the original polymer formulation. Such a material would be suitable in applications requiring mechanically robust but flexible polyurethanes such as catheters, sealants, and cardiovascular implants. This study demonstrated a unique and versatile modification scheme not yet reported previously in the literature. Some advantages of this modification scheme were made apparent by a marked improvement in thermal degradation and nanoparticle dispersion in the selected polymer matrix, two highly sought after features concerning cellulose nanomaterials. Additionally, this functionalization method may serve as a platform for the addition of other desirable functional groups and/or as a means for increasing compatibility with a range of organic solvents and polymers. The isocyanate-functional CNCs could be used in epoxy formulations utilizing amine cross-linkers, where the CNCs would be covalently bonded to the matrix. Another interesting route could explore additional modification steps involving hydroxyl- or amine-functional monomers that contain vinyl groups for thermoplastic CNC composites produced by free radical polymerization. Overall, the functionalization scheme presented is anticipated to be useful in a range of applications not limited to the composite application presented here.

■ ASSOCIATED CONTENT

Supporting Information

The Supporting Information is available free of charge on the ACS Publications website at DOI: 10.1021/acsami.5b10723.

TEM image of CNCs used in this work, FTIR spectra of toluene supernatant after sufficient washing of the reaction product, polarized optical micrographs comparing the level of dispersion obtained with the um-CNC/polyurethane composites produced with DMSO and toluene, details of the DS and DS_{surf} calculation, ^{13}C NMR spectra of the IPDI molecule used in this work, a representative tensile stress versus tensile strain curve for the matrix and composites, and a tabled summary of the mechanical properties of the polyurethanes synthesized in this work. (PDF)

■ AUTHOR INFORMATION

Corresponding Author

*Phone: 404.385.2151. Fax: 404.894.2866. E-mail: carson.meredith@chbe.gatech.edu.

Notes

The authors declare no competing financial interest.

■ ACKNOWLEDGMENTS

The authors of this paper would like to thank the USDA Forest Products Laboratory (FPL) for their financial support and collaboration. The authors thank J. Leisen of Georgia Inst. of Technology for the NMR measurements and discussions, Prof. E. Mintz of Clark Atlanta Univ. for useful discussions, D. Sherman of DS imaging West Lafayette, IN, for the TEM imaging of the CNCs, and R. Reiner and A. Rudie of the Forest Products Laboratory, Madison, WI, for providing CNCs for this research.

■ REFERENCES

(1) Moon, R. J.; Martini, A.; Nairn, J.; Simonsen, J.; Youngblood, J. Cellulose nanomaterials review: structure, properties and nanocomposites. *Chem. Soc. Rev.* **2011**, *40*, 3941−3994.

(2) Habibi, Y.; Lucia, L. A.; Rojas, O. J. Cellulose Nanocrystals: Chemistry, Self-Assembly, and Applications. *Chem. Rev.* **2010**, *110*, 3479−3500.

(3) *Agenda 2020, Technology Alliance Critical Nanotechnology Needs in the Forest Products Industry White Paper;* 2009.

(4) Anglès, M. N.; Dufresne, A. Plasticized Starch/Tunicin Whiskers Nanocomposite Materials. 2. Mechanical Behavior. *Macromolecules* **2001**, *34* (i), 2921−2931.

(5) Hu, Z.; Patten, T.; Pelton, R.; Cranston, E. D. Synergistic Stabilization of Emulsions and Emulsion Gels with Water-Soluble Polymers and Cellulose Nanocrystals. *ACS Sustainable Chem. Eng.* **2015**, *3*, 1023−1031.

(6) Junior de Menezes, A.; Siqueira, G.; Curvelo, a. a S.; Dufresne, A. Extrusion and characterization of functionalized cellulose whiskers reinforced polyethylene nanocomposites. *Polymer* **2009**, *50*, 4552−4563.

(7) Dash, R.; Ragauskas, A. J. Synthesis of a novel cellulose nanowhisker-based drug delivery system. *RSC Adv.* **2012**, *2*, 3403−3409.

(8) Liu, A.; Berglund, L. a. Fire-retardant and ductile clay nanopaper biocomposites based on montmorrilonite in matrix of cellulose nanofibers and carboxymethyl cellulose. *Eur. Polym. J.* **2013**, *49*, 940−949.

(9) Hu, Z.; Ballinger, S.; Pelton, R.; Cranston, E. D. Surfactant-enhanced cellulose nanocrystal Pickering emulsions. *J. Colloid Interface Sci.* **2015**, *439*, 139−148.

(10) Tang, J.; Lee, M. F. X.; Zhang, W.; Zhao, B.; Berry, R. M.; Tam, K. C. Dual responsive pickering emulsion stabilized by poly[2-(dimethylamino) ethyl methacrylate] grafted cellulose nanocrystals. *Biomacromolecules* **2014**, *15*, 3052−3060.

DOI: 10.1021/acsami.5b10723
ACS Appl. Mater. Interfaces 2016, 8, 1458−1467

(11) Gardner, D. J.; Oporto, G. S.; Mills, R.; Azizi Samir, M. A. S. Adhesion and surface issues in cellulose and nanocellulose. *J. Adhes. Sci. Technol.* **2008**, *22*, 545−567.
(12) Eyley, S.; Thielemans, W. Surface modification of cellulose nanocrystals. *Nanoscale* **2014**, *6*, 7764−7779.
(13) Kargarzadeh, H.; Sheltami, R. M.; Ahmad, I.; Abdullah, I.; Dufresne, A. Cellulose nanocrystal: A promising toughening agent for unsaturated polyester nanocomposite. *Polymer* **2015**, *56*, 346−357.
(14) Rueda, L.; Fernández d'Arlas, B.; Zhou, Q.; Berglund, L. A.; Corcuera, M. A.; Mondragon, I.; Eceiza, A. Isocyanate-rich cellulose nanocrystals and their selective insertion in elastomeric polyurethane. *Compos. Sci. Technol.* **2011**, *71*, 1953−1960.
(15) Moore, M. G. *The Economic Benefits of the U.S. Polyurethanes Industry 2013;* American Chemistry Council, 2014.
(16) Zhang, C.; Madbouly, S. a; Kessler, M. R. Biobased polyurethanes prepared from different vegetable oils. *ACS Appl. Mater. Interfaces* **2015**, *7*, 1226−1233.
(17) Kucinska-Lipka, J.; Gubanska, I.; Janik, H.; Sienkiewicz, M. Fabrication of polyurethane and polyurethane based composite fibres by the electrospinning technique for soft tissue engineering of cardiovascular system. *Mater. Sci. Eng., C* **2015**, *46*, 166−176.
(18) Kresta, J. *60 Years of Polyurethanes;* University of Detroit Mercy, 1998; pp 26−29.
(19) Liff, S. M.; Kumar, N.; McKinley, G. H. High-performance elastomeric nanocomposites via solvent-exchange processing. *Nat. Mater.* **2007**, *6*, 76−83.
(20) Sen, R.; Zhao, B.; Perea, D.; Itkis, M. E.; Hu, H.; Love, J.; Bekyarova, E.; Haddon, R. C. Preparation of single-walled carbon nanotube reinforced polystyrene and polyurethane nanofibers and membranes by electrospinning. *Nano Lett.* **2004**, *4*, 459−464.
(21) Xia, H.; Song, M. Preparation and characterization of polyurethane−carbon nanotube composites. *Soft Matter* **2005**, *1*, 386−394.
(22) Cai, D.; Yusoh, K.; Song, M. The mechanical properties and morphology of a graphite oxide nanoplatelet/polyurethane composite. *Nanotechnology* **2009**, *20*, 1−5.
(23) Saralegi, a.; Rueda, L.; Martin, L.; Arbelaiz, a.; Eceiza, a.; Corcuera, M. a. From elastomeric to rigid polyurethane/cellulose nanocrystal bionanocomposites. *Compos. Sci. Technol.* **2013**, *88*, 39−47.
(24) Li, Y.; Ren, H.; Ragauskas, A. J. Rigid Polyurethane Foam/Cellulose Whisker Nanocomposites: Preparation, Characterization, and Properties. *J. Nanosci. Nanotechnol.* **2011**, *11*, 6904−6911.
(25) Meier-Westhues, U. *Polyurethanes, Coatings, Adhesives and Sealants;* Vincentz Network: Hannover, 2007; pp 52−55.
(26) *Wood Floor Coating Technology Comparison Bayer MaterialScience publication No. 20937*; Bayer MaterialScience, 2012.
(27) Ono, H.-K.; Jones, F. N.; Pappas, S. P. Relative Reactivity of Isocyanate Groups of Isophorone Diisocyanate. Unexpected High Reactivity of the Secondary Isocyanate Group. *J. Polym. Sci., Polym. Lett. Ed.* **1985**, *23*, 509−515.
(28) Götz, H.; Beginn, U.; Bartelink, C. F.; Grünbauer, H. J. M.; Möller, M. Preparation of isophorone diisocyanate terminated star polyethers. *Macromol. Mater. Eng.* **2002**, *287*, 223−230.
(29) Marschner, M.; Ritter, W. ^{13}C NMR studies on the relative reactivity of isocyanate groups of isophorone diisocyanate isomers. *Macromol. Chem. Phys.* **1990**, *191*, 1843−1852.
(30) Lomölder, R.; Plogmann, F.; Speier, P. Selectivity of isophorone diisocyanate in the urethane reaction influence of temperature, catalysis, and reaction partners. *J. Coat. Technol.* **1997**, *69*, 51−57.
(31) Beck-Candanedo, S.; Roman, M.; Gray, D. G. Effect of reaction conditions on the properties and behavior of wood cellulose nanocrystal suspensions. *Biomacromolecules* **2005**, *6*, 1048−1054.
(32) Girouard, N.; Schueneman, G. T.; Shofner, M. L.; Meredith, J. C. Exploiting colloidal interfaces to increase dispersion, performance, and pot-life in cellulose nanocrystal/waterborne epoxy composites. *Polymer* **2015**, *68*, 111−121.
(33) Miller, A. P. Lange's Handbook of Chemistry. In *American Journal of Public Health and the Nations Health;* **1941**; Vol. *31*, p 1324.
(34) Gårdebjer, S.; Bergstrand, A.; Idström, A.; Börstell, C.; Naana, S.; Nordstierna, L.; Larsson, A. Solid-state NMR to quantify surface coverage and chain length of lactic acid modified cellulose nanocrystals, used as fillers in biodegradable composites. *Compos. Sci. Technol.* **2015**, *107*, 1−9.
(35) Abdalla, A. I.; Ragab, Y. A. Esterification of Shambat Cotton Cellulose by (octanoyl (C8), decanoyl (C10) and lauroyl (C12) acid chlorides using *N,N*-Dimethyl Acetamide/ Lithium Chloride Solvent System. *International Journal of Advanced Research in Biological Sciences* **2014**, *1*, 101−112.
(36) Wu, X.; Moon, R. J.; Martini, A. Crystalline cellulose elastic modulus predicted by atomistic models of uniform deformation and nanoscale indentation. *Cellulose* **2013**, *20*, 43−55.
(37) Park, S.; Baker, J. O.; Himmel, M. E.; Parilla, P. A.; Johnson, D. K. Cellulose crystallinity index: measurement techniques and their impact on interpreting cellulase performance. *Biotechnol. Biofuels* **2010**, *3*, 10.
(38) Park, S.; Johnson, D. K.; Ishizawa, C. I.; Parilla, P. a.; Davis, M. F. Measuring the crystallinity index of cellulose by solid state 13C nuclear magnetic resonance. *Cellulose* **2009**, *16*, 641−647.
(39) Larsson, P. T.; Wickholm, K.; Iversen, T. A CP/MAS 13C NMR investigation of molecular ordering in celluloses. *Carbohydr. Res.* **1997**, *302*, 19−25.
(40) Cho, G.; Natansohn, A.; Ho, T.; Wynne, K. J. Phase Structure of Poly (dimethylsiloxane-urea-urethane) - Segmented Copolymers as Observed by Solid-State Nuclear Magnetic Resonance Spectra. *Macromolecules* **1996**, *29*, 2563−2569.
(41) Peng, Y.; Gardner, D. J.; Han, Y.; Kiziltas, A.; Cai, Z.; Tshabalala, M. a. Influence of drying method on the material properties of nanocellulose I: Thermostability and crystallinity. *Cellulose* **2013**, *20*, 2379−2392.
(42) Pereda, M.; Kissi, N. El; Dufresne, A. Extrusion of polysaccharide nanocrystal reinforced polymer nanocomposites through compatibilization with poly(ethylene oxide). *ACS Appl. Mater. Interfaces* **2014**, *6*, 9365−9375.
(43) Kargarzadeh, H.; Ahmad, I.; Abdullah, I.; Dufresne, A.; Zainudin, S. Y.; Sheltami, R. M. Effects of hydrolysis conditions on the morphology, crystallinity, and thermal stability of cellulose nanocrystals extracted from kenaf bast fibers. *Cellulose* **2012**, *19*, 855−866.
(44) Rämänen, P.; Penttilä, P. a.; Svedström, K.; Maunu, S. L.; Serimaa, R. The effect of drying method on the properties and nanoscale structure of cellulose whiskers. *Cellulose* **2012**, *19*, 901−912.
(45) Rao, Y.; Munro, J.; Ge, S.; Garcia-Meitin, E. PU elastomers comprising spherical nanosilicas: Balancing rheology and properties. *Polymer* **2014**, *55*, 6076−6084.
(46) Cheng, Q.; Wang, S.; Rials, T. G. Poly(vinyl alcohol) nanocomposites reinforced with cellulose fibrils isolated by high intensity ultrasonication. *Composites, Part A* **2009**, *40*, 218−224.
(47) Xu, S.; Girouard, N.; Schueneman, G.; Shofner, M. L.; Meredith, J. C. Mechanical and thermal properties of waterborne epoxy composites containing cellulose nanocrystals. *Polymer* **2013**, *54*, 6589−6598.
(48) Chen, Y.; Zhou, S.; Yang, H.; Wu, L. Structure and properties of polyurethane/nanosilica composites. *J. Appl. Polym. Sci.* **2005**, *95*, 1032−1039.
(49) Fu, S. Y.; Feng, X. Q.; Lauke, B.; Mai, Y. W. Effects of particle size, particle/matrix interface adhesion and particle loading on mechanical properties of particulate-polymer composites. *Composites, Part B* **2008**, *39*, 933−961.

DOI: 10.1021/acsami.5b10723
ACS Appl. Mater. Interfaces 2016, 8, 1458−1467